SCIENCE CHINA
Chemistry

•ARTICLES•

August 2021 Vol.64 No.8: 1389–1400
https://doi.org/10.1007/s11426-020-1009-y

Hierarchically porous polymers with ultra-high affinity for bisphenol A enables high efficient water purification

Zelun Li[1†], Juan Wang[1†], Qian Chen[1], Kelong Ai[2*] & Lehui Lu[1*]

[1]*State Key Laboratory of Electroanalytical Chemistry, Changchun Institute of Applied Chemistry, Chinese Academy of Sciences, Changchun 130022, China;*
[2]*Department of Pharmacology, Xiangya School of Pharmaceutical Sciences, Central South University, Changsha 410078, China*

Received December 3, 2020; accepted April 13, 2021; published online June 29, 2021

The widespread use of bisphenol A (BPA) poses a serious threat to the environment and human health. However, efficient removal of BPA in water is incredibly challenging, owing to the inert chemical nature and electrical neutrality of BPA. In order to solve this problem, for the first time, we propose that a strategy of designing conjugated porous polymers with the pore size matching the size of BPA can greatly enhance the binding force of BPA. On this basis, we developed a novel conjugated poly 1,3,5-tri[4-(diphenylamino)phenyl]benzene (MPDPB) with intrinsic pore matching the size of BPA and multi-stage porous structure by editing polymerization with nitrobenzene. The binding energy of MPDPB to BPA is the highest at present (37.84 kcal/mol), which is 2.3 times that of the most powerful adsorbent previously reported and five times that of the conventional adsorbent. These advantages make MPDPB have super-high adsorption performance towards BPA and high absorbing stability under extreme environments. Impressively, MPDPB could be easily loaded on a non-woven fabric to generate point-of-use devices, which could eliminate more than 99.8% of BPA, making it the best BPA candidate adsorbent material. We believe that the proposed material design derived from the specific structure of the contaminant molecule can be extended to exploring further innovative adsorbents.

bisphenol A, porous polymer, water purification, adsorbent, micropollutant

Citation: Li Z, Wang J, Chen Q, Ai K, Lu L. Hierarchically porous polymers with ultra-high affinity for bisphenol A enables high efficient water purification. *Sci China Chem*, 2021, 64: 1389–1400, https://doi.org/10.1007/s11426-020-1009-y

1 Introduction

Premature death from environmental pollution accounts for more than 16% of the total death [1]. Chemical pollution is among the most serious and widespread environmental problems. Bisphenol A (BPA) is a chemical material widely used in many manufacturing industries such as tanning materials, paper, electronic products, toys, containers, with an annual global output of more than 8 million tons and at an increasing rate of 6% per year [2,3]. Recent evidence has revealed that BPA is an estrogen analog that has impacts on the reproductive and cardiovascular systems, and can elicit deleterious effects to the human body at extremely low concentration, especially for young children [4–8]. It will rapidly spread once BPA leaks into the water, thus leading to a significant threat to the environment and human health. A recent study has indicated that BPA exists in the blood of more than 86% of adults [9]. Adsorption has received significant attention for the advantages of economy and no subsequent pollution over other water purification approaches [10,11]. However, BPA is a kind of electrically neutral organic small molecule, and its chemical properties are quite stable without a strong binding site. Therefore, it

†These authors contributed equally to this work.
*Corresponding authors (email: aikelong@csu.edu.cn; lehuilu@ciac.ac.cn)

remains incredibly challenging for current adsorbent materials to effectively remove BPA from water. To date, numerous efforts have been devoted to developing new adsorbent materials for BPA adsorption, such as metal organic frameworks (MOF), covalent organic frameworks (COF), and porous polymers [10,12–21]. Despite recent progress, current absorbents for BPA still face hurdles for practical applications.

Among many factors affecting the performance of adsorbents, the affinity of absorbents to BPA is the most fundamental factor. However, previous studies have seldom focused on this crucial fundamental issue. The main reason is that the electroneutrality and chemical inertia of BPA makes it very difficult to improve the affinity of BPA. Therefore, there is an urgent need to develop a novel effective strategy for the removal of BPA in water. We believe that an ideal BPA adsorbent material should satisfy the following two points: (1) high binding ability towards BPA for improving removal efficiency; (2) multi-stage porous structure that can facilitate the exposure of internal absorbing sites to BPA and subsequently increase the adsorption rate and capacity. Nevertheless, to the best of our knowledge, there is no such adsorbent that can meet these criteria at present.

Since BPA is relatively chemically inert, increasing the van der Waals force between the adsorbent material and BPA could, therefore, enhance the adsorbing performance of adsorbents. Notably, almost all current adsorbents are not designed according to the characteristics of BPA. For instance, cyclodextrin, the most powerful adsorbents at present, has a cavity structure (0.61 nm) that could increase its van der Waals force with BPA, contributing to its higher adsorption capacity compared with other adsorbent materials [12]. Nevertheless, the cavity is too large to match well with the chemical structure of BPA, resulting in suboptimal binding energy. On the other hand, BPA cannot enter the pore if the pore size is too small, and thus greatly reduce the adsorption efficiency. For example, the pore size of COP-99 is 0.51 nm, which exhibits low removal efficiency for BPA [15].

Herein, we report an innovative multi-stage porous polymer, poly(1,3,5-tris[4-(diphenylamino)phenyl]benzene) (MPDPB) composed of total chemical inert bonds, with a theoretical pore size (0.59 nm) that matches well with the physical size of BPA (Scheme 1). On the one hand, the conjugated structure can significantly enhance the van der Waals force between polymer and BPA. On the other hand, the size-matching pores can greatly increase contact between BPA and the pore wall, further strengthening the van der Waals interaction between them. Another unique feature of this strategy is that nitrobenzene is used as a porogenic agent for editing MPDPB. With this strategy, MPDPB with extended BPA-matched endogenous micropores and other pore structures is successfully prepared. Theoretical calculations and experiments have shown that the binding energy of the polymer to BPA is much larger than those of cyclodextrin-based adsorbents and the most commonly used activated carbon. The maximum adsorption capacity of MPDPB to BPA is determined to be 826 mg/g, which is the highest value among the reported literature. Comparable removal efficiency (highest efficiency of 99.8% and average efficiency of 96.3%) of MPDPB has been achieved for the removal of other contaminants. Impressively, MPDPB was developed into a cost-effective platform for point-of-use water purification at any geographical place.

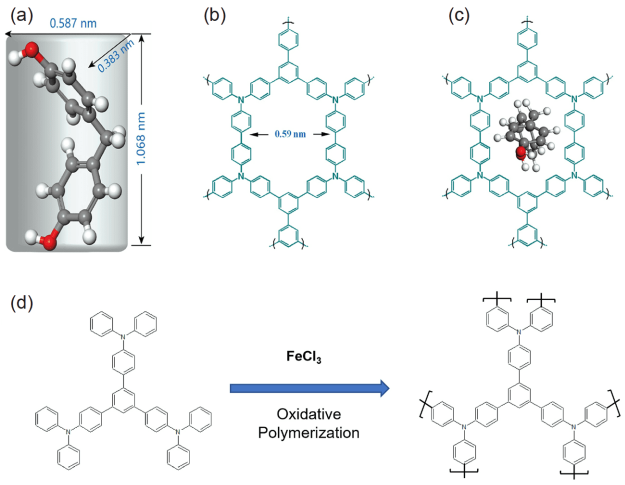

Scheme 1 Schematic illustration of (a) molecular structure of bisphenol A, (b) MPDPB, and (c) size-matched interaction between bisphenol A and MPDPB, (d) preparation of MPDPB from the monomer (color online).

2 Experimental

2.1 Preparation of DPB monomer

1,3,5-Tris(4-iodophenyl)benzene (4.2 g), diphenylamine (6.24 g), KOH pellets (6.21 g), copper bronze (3.7 g), and *n*-decane (30 mL) were placed in a two-necked flask equipped with a water condenser and Ar gas supply [22]. The reaction mixture was refluxed with an oil bath for 48 h or until only one product spot could be detected by thin layer chromatography (TLC). The reaction mixture was then allowed to cool, followed by the addition of methanol (200 mL), which precipitated the crude product. The solid was filtered off, dissolved in CH_2Cl_2 and filtered to remove inorganic residues. The product was purified by flash chromatography on silica gel. Light petroleum-CH_2Cl_2 (95:5) eluted the 1,3,5-tris[4-(diphenylamino)phenyl]benzene (DPB) (3 g, 55%) as white powders.

2.2 Synthesis of the MPDPB

0.3 g of the DPB monomer was dispersed in 30 mL of chloroform, and then mixed with 1.2 g of anhydrous ferric

chloride dispersed in 5 mL of nitrobenzene. The mixture in the reaction kettle was kept at 40 °C for 3 days. Methanol (contains 2 M HCl) was used to wash the product 4 times, and deionized water was used to wash the product 4 times. MPDPB was given by lyophilization.

2.3 Synthesis of the PDPB

0.3 g of DPB monomer was dissolved into 35 mL of chloroform, 1.2 g of anhydrous ferric chloride was then added into the mixture. The mixture in the reaction kettle was kept at 40 °C for three days. Methanol (contains 2 M HCl) was used to wash the product 4 times, and deionized water was used to wash the product 4 times. PDPB was given by lyophilization.

2.4 Synthesis of the β-cyclodextrin-based material (CD)

CD adsorbent was obtained by simple modification of previous literature [12]. Argon was introduced into 40 mL tetrahydrofuran, then 0.5 g of tetrafluoroterephthalic acid, 1 g of beta-cyclohexane and 1.5 g of potassium carbonate were added, and stirred for 2 days at 85 °C. Yellow solids were filtered and washed with deionized water, tetrahydrofuran and dichloromethane, respectively. Finally, CD adsorbent was obtained by freeze-drying.

2.5 Experimental conditions for adsorption

Adsorption capacity of various adsorbents towards BPA: BPA removal experiments were determined at room temperature with a stirring rate of 260 r/min. The concentration of each adsorbent (MPDPB, PDPB, CD, AC) is 1 mg/mL. 10 mg of absorbent was stirred in the aqueous solution of BPA (0.1 mM, 10 mL) for 10 s, 30 s, 1 min, 2 min, 5 min and 10 min, 30 min, and 60 min, respectively, followed by pushing the suspension using a syringe with a Whatman 0.2 μm inorganic membrane filter. The filtrate was tested *via* UV-vis spectroscopy. The concentrations of aqueous solution of various pollutants are as follows: 0.1 mM of BPS; 0.04 mM of ethinyl oestradiol; 0.1 mM of 1-NA; 0.1 mM of 2-NO; 0.1 mM of metolachlor; 0.08 mM of propranolol hydrochloride; 0.1 mM of methyl orange and 0.1 mM of methylene blue. The concentration of MPDPB is 1 mg/mL. 10 mg of absorbent was stirred in the aqueous solution of pollutants (10 mL) for 10 s, 30 s, 1 min, 2 min, 5 min and 10 min, 30 min, and 60 min, respectively, followed by pushing the suspension using a syringe with a Whatman 0.2 μm inorganic membrane filter. The filtrate was tested *via* UV-vis spectroscopy. The adsorption experiments were conducted under room temperature with a stirring rate of 260 r/min. Adsorption experiments of the point-of-use device: a wastewater sample containing 20 ppm BPA was used to test the purifiers. The filtrate was tested *via* mass spectrometry (HPLC-MS). The adsorption experiments were conducted at room temperature. Adsorption experiment of simulated environmental wastewater sample: 100 μg/L of BPA, 2.5 μg/L of BPS, 50 μg/L of ethinyl oestradiol, 25 μg/L of 2-NO, 5 μg/L of metolachlor, 100 μg/L of propranolol, 5 μg/L of 1-NA, 100 μg/L of methyl orange and 100 μg/L of methylene blue were used to simulate environmental wastewater. Then the mixture was passed through the simple purifier. HPLC-MS was used to determine the removal efficiency of the adsorbent. The adsorption experiment was conducted at room temperature.

2.6 MPDPB regeneration experiments

MPDPB (25.00 mg) was firstly soaked in 25 mL of deionized water for 10 min, and the wet product was filtered by using a Whatman filter paper. The product was added into a round-bottomed flask (50 mL), mixing with 25 mL of the solution of BPA (0.1 mM). The polymer was filtered using a Whatman filter paper after the mixture was stirred for 30 min. UV-vis spectroscopy was utilized to test the residual concentration of the solution of bisphenol A. MPDPB was regenerated through soaking in 50 mL of MeOH for one day and then recovering by filtration. The MPDPB was dry in the oven at 70 °C.

2.7 Construction of non-woven fabric for water purification

A piece of medical non-woven fabric was immersed in the ethanol solution of MPDPB, and dried under ambient condition to obtain the non-woven fabric for water purification.

2.8 Removal efficiency

The efficiency of organic micropollutants by MPDPB was calculated as follows:

$$\text{Pollutant removal efficiency (\%)} = \frac{C_0 - C_t}{C_0} \times 100\%$$

where C_0 (mM) and C_t (mM) are the preliminary and residual concentrations of the organic micropollutants, respectively. The number of organic micropollutants entered into the MPDPB was calculated as follows:

$$q_t = \frac{(C_0 - C_t)M_w}{m}$$

where q_t (mg/g) is the amount of organic micropollutant adsorbed per gram of adsorbent MPDPB at time t (min), C_0 (mmol/L) represents the preliminary concentration of organic micropollutants in the solution, and C_t (mmol/L) represents the residual concentrations of organic

micropollutants in the filtrates. M_w (g/mol) represents the molar mass of the organic micropollutants. m (g) is the mass of MPDPB prepared in this work.

2.9 Pseudo-second-order model

The uptake rate of MPDPB used in this study was determined by the model of Ho and McKay's pseudo-second-order, from which the apparent rate constant K_{obs} can be calculated:

$$\frac{t}{q_t} = \frac{t}{q_e} + \frac{1}{K_{obs} q_e^2}$$

where q_t and q_e represent the organic micropollutants (mg adsorbate per g MPDPB) at time t (min) and at equilibrium, respectively. K_{obs} (g mg^{-1} min^{-1}) can be obtained from linear fitting of the plot of t/q_t versus t by Origin 8. All the experiments were conducted at room temperature.

2.10 The Langmuir adsorption isotherm

The uptake rate of MPDPB was determined by the Langmuir adsorption isotherm, which is established by plotting $1/q_e$ versus $1/c$ according to the following equation:

$$\frac{1}{q_e} = \frac{1}{q_{max,e}} + \frac{1}{q_{max,e} K_c}$$

where q_e represents the organic micropollutants (mg adsorbate per g MPDPB) at equilibrium. $q_{max,e}$ (mg adsorbate per g MPDPB) represents the maximum adsorption amount of the MPDPB at equilibrium. c (mol L^{-1}) represents the residual organic micropollutants concentration at equilibrium. K (L mol^{-1}) represents the equilibrium constant.

2.11 The distribution coefficient (K_d) value

The distribution coefficient (K_d) value is defined as:

$$K_d = \left(\frac{C_0 - C_e}{C_e}\right) \times \frac{V}{m}$$

where V is the volume of the treated solution (mL), m is the weight of used adsorbent (g), C_0 is the initial concentration of BPA, and C_e is the final equilibrium concentration of BPA. In the present work, 25 mL aqueous solution of BPA was treated by 25.0 mg adsorbent for 2 h. The initial concentration of BPA was 22.8 ppm.

2.12 QCM measurement

A 5-MHz AT-cut quartz plate equipped with a gold electrode was employed as the QCM resonator. The gold electrode was cleaned with ethanol and deionized water, and drying under a nitrogen atmosphere. The QCM measurement was carried out at room temperature, using a flow rate of 20 μL/min. The gold electrode was cleaned by a mixture of hydrogen peroxide, ammonia and deionized water (1:1:5) and dried using purified nitrogen. The shear modulus (μ) and shear viscosity (η) were determined by the Q-Tools program. The QCM data were collected by the change of the 35-MHz seventh overtone of the fundamental frequency (5 MHz) after the sequential addition of the BPA aqueous solution (0.1 ppb) to a gold electrode. The change in frequency was related to the mass change, which is determined to be 9.35 ng/cm^2 using the following Sauebrey equation:

$$\Delta m = -17.7 \times \Delta f / n$$

where Δm is the mass change, Δf is the frequency change, n is the number of the harmonics of the fundamental resonance frequency adopted in the study.

2.13 Fluorescence microscopy measurement

Leica DMI4000B inverted biological microscope was used to obtain the fluorescence microscopic images. Briefly, HeLa cells MPDPB were seeded into a 6-well cell culture plate with high-glucose DMEM medium and fetal bovine serum (10%), culturing with the atmosphere of CO_2 (5%) and 95% air at 37 °C for 24 h. After washing with phosphate buffer saline (PBS) twice, HeLa cells were incubated with 2 mg/mL MPDPB for 24 h. The cells were stained with both calcein AM (calcein acetoxymethyl ester) and PI (propidium iodide).

2.14 Cell cytotoxicity test

HeLa cells were used to perform the methyl thiazolyl tetrazolium (MTT) assays to assessing the *in vitro* cytotoxicity. Briefly, HeLa cells were seeded into a 96-well cell culture plate with high-glucose DMEM medium and fetal bovine serum (10%), culturing with the atmosphere of CO_2 (5%) and 95% air at 37 °C for 24 h. After washing with PBS twice, HeLa cells were incubated with MPDPB with different concentrations for 24 h. After washing with PBS twice, 100 μL of the diluted solution of methyl thiazolyl tetrazolium was added into each well of the 96-well cell culture plate, culturing with the atmosphere of CO_2 (5%) and 95% air at 37 °C for 4 h. 100 μL of dimethyl sulfoxide (DMSO) was added into each well of the 96-well cell culture plate after the supernatant was moved by a syringe. The 96-well cell culture plate was shaking for 15 min. Nano Quant microplate reader was used to determine the absorbance at 570 nm to measure the cell viability.

3 Results and discussion

3.1 Synthesis and characterization of MPDPB

1,3,5-Tris[4-(diphenylamino)phenyl] benzene (denoted as DPB monomer), was obtained by catalytic reaction of 1,3,5-

tris(4-iodophenyl)-benzene and diphenylamine using copper bronze as the catalyst (Figures S1, S2, Supporting Information online). Usually, surfactants, amphoteric polymers and inorganic oxides are used as templates to prepare porous materials. These methods are often inefficient and require the removal of unnecessary impurities from complex operations such as templates. In order to solve these shortcomings, we developed a new way to obtain MPDPB with a multi-stage porous structure by a special two-solvent system (Figure 1 (a)). We dissolved oxidants in nitrobenzene because $FeCl_3$ can dissolve well in nitrobenzene but have little solubility in chloroform. Similarly, DPB monomers are well soluble in chloroform but less soluble in nitrobenzene. DPB monomer contains three triphenylamine molecules. It is well known that Fe^{3+} is a strong oxidant, hence triphenylamine is easily oxidized by Fe^{3+} and polymerized to form polymers [23,24]. Therefore, in the presence of Fe^{3+}, the DPB monomer is easily oxidized and polymerized with the surrounding DPB monomer. Once the nitrobenzene solution of oxidant was fully mixed with chloroform solution containing DPB monomer, DPA would polymerize along the periphery of the nitrobenzene nano-droplets rich in oxidant to form MPDPB polymer. Here nitrobenzene was used as a good pore-forming agent to efficiently edit MPDPB synthesis, so as to ingeniously obtain MPDPB with a multi-stage pore structure. Then the residual nitrobenzene and iron impurities can be removed simply by washing with water and methanol (2 M HCl). After the reaction, the white DPB monomer was polymerized to form brownish yellow MPDPB powders. The MPDPB polymer is insoluble in chloroform (DPB is easily soluble in chloroform), which further illustrated the successful polymerization. X-ray photoelectron spectroscopy (XPS) measurement confirmed that Fe impurities can be successfully removed after purification (Figure S3).

To further demonstrate the unique features of this two-solvent system, we also synthesized poly-1,3,5-tris[4-(diphenylamino)phenyl]benzene (PDPB) without nitrobenzene as the reference. N_2 adsorption-desorption curve illustrated that the specific surface area of MPDPB is 1383 m^2/g, which is larger than that of PDPB (795 m^2/g) (Figure 1(b)). Moreover, MPDPB demonstrated a relatively larger hysteresis loop with a mesoporous structure (2–25 nm). Also, both MPDPB and PDPB illustrated an intrinsic pore size of 0.59 nm (Figure 1(c)), while MPDPB depicted a more mesoporous structure, which was mainly derived from the pore-forming effect of nitrobenzene during the synthesis. This unique pore structure of MPDPB can not only ensure that MPDPB adsorbs a wide range of organic pollutants with different sizes, but also act as a good high-speed channel for pollutant transport, thus greatly improving the adsorption kinetics of the removal of water pollution and ensuring the excellent adsorption performance of the adsorbent.

Fourier transform infrared spectroscopy (FTIR) of MPDPB was measured. MPDPB contains strong benzene ring vibration at 1,490 cm^{-1} and –OH vibration (water molecule adsorbed by MPDPB) at 3,355 cm^{-1}, but lacks the vibration of $–CH_3$, indicating that MPDPB has a good conjugated structure (Figure S4). We compared the C–H bond in the benzene of DPB with the C–H bond in the benzene of MPDPB. As shown in the FTIR spectrum (Figure S5), the

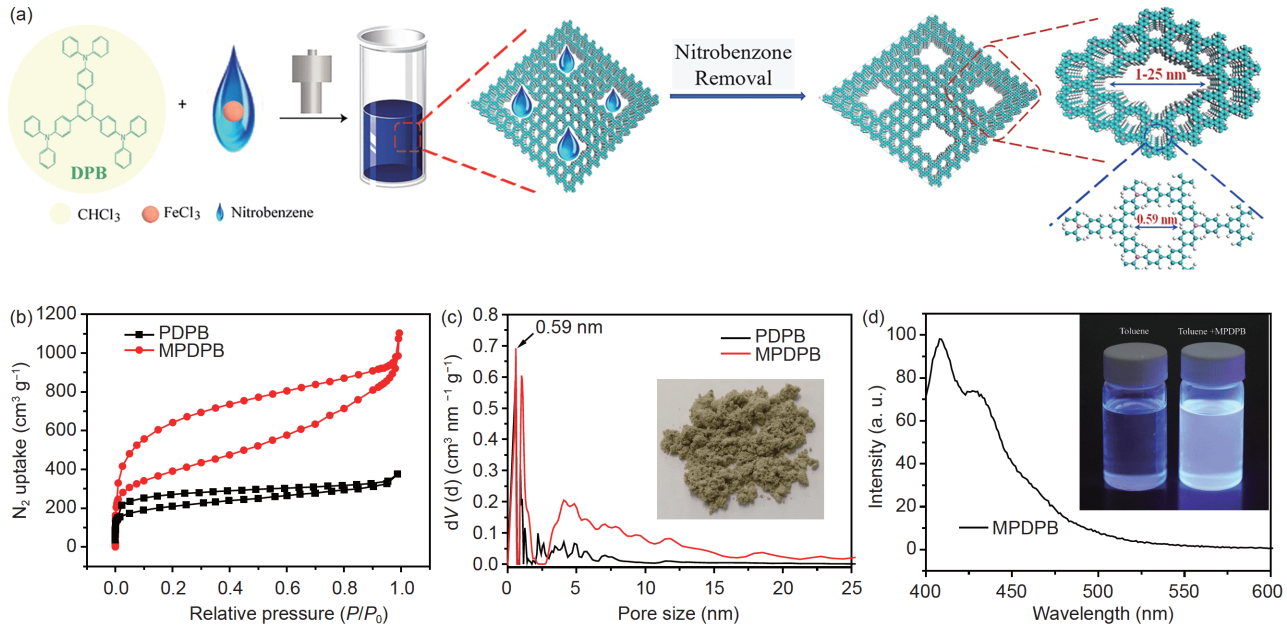

Figure 1 (a) Schematic illustration of the preparation of MPDPB under a nitrobenzene-chloroform double solvent system. (b) N_2 adsorption-isotherm of PDPB and MPDPB. (c) Pore width distribution of PDPB and MPDPB, inset is the image of MPDPB power. (d) The fluorescence spectrum of MPDPB, inset is the fluorescence images of MPDPB under the irradiation of ultraviolet lamp, the left is toluene, and the right is toluene with MPDPB (color online).

C–H bond in the benzene located at 3,028 cm^{-1} of DPB is much lower than that of MPDPB, indicating the successful polymerization. We further analyzed MPDPB *via* XPS. MPDPB mainly contains three elements (Figure S3), which are C, N and O. Among them, O is caused by water adsorbed by MPDPB. The fine structure of C 1s is analyzed. It is found that XPS of C 1s is mainly located at 284.6 and 285.6 eV, which belong to aromatic ring carbon and C–N bonds, respectively (Figure S6a). Fine XPS analysis of N 1s showed that it was located at 399.7 eV, which was mainly attributed to tertiary amine structure (Figure S6b). We also analyzed the solid-state NMR of MPDPB, and found that the main carbon chemical shift peaks of MPDPB were between 126.8 and 146.3 ppm (Figure S7), of which 126.8 ppm was mainly the carbon shift of conjugated benzene rings, while 146.3 ppm was caused by the high field shift of carbon due to the electron-rich N-bonding in benzene rings. Through the result of the ultraviolet absorption spectrum, we found that MPDPB has absorption at 345.6 nm (Figure S8), which is attributed to the n→π* transition of the conjugated biphenyl group in the structure of MPDPB. The conjugated structure in MPDPB may demonstrate unique fluorescence properties. To this end, we investigated its fluorescence properties. As shown in Figure S9, the fluorescence excitation and emission spectrums of MPDPB exhibit good mirror symmetry and emit strong blue fluorescence under the irradiation of ultraviolet lamp (Figure 1(d)), illustrating that MPDPB can be used as a good marker in the field of pollutant detection. Through the above experiments, we concluded that MPDPB has an endogenous conjugated pore structure matching the size of BPA, which can greatly improve the affinity of BPA.

3.2 Affinity of MPDPB for BPA

It is well-known that affinity is the most fundamental factor affecting the performance of adsorbents. To assess the affinity, MPDPB was mixed with BPA in an aqueous solution. The interaction between MPDPB and BPA was obtained after 1 min. Firstly, Compared with MPDPB, MPDPB adsorbed BPA showed a new $–CH_3$ vibration at 2,967 cm^{-1} and a stronger –OH vibration at 3,355cm^{-1} (Figure S4) in FTIR spectrum. This indicates that MPDPB can bind with BPA rapidly and efficiently within 1 min, resulting in the characteristic FITR vibration of BPA. Further XPS analysis showed that there was a stronger peak of O from BPA after adsorbing BPA, synergistic indicating that MPDPB could rapidly bind to BPA in an aqueous solution (Figure S10). The affinity between BPA and MPDPB can also be proved through TGA experiments. As Figure S11 depicts, BPA gradually melts and boils with the increase of temperature, and finally loses all the weight around 263 °C when BPA is heated in the air. We reasoned that the high affinity of MPDPB with BPA can effectively capture BPA molecules, and thus preventing the escaping of BPA under high temperature. Therefore, in this binding system, the total weight loss temperature of BPA is 337 °C, which is much higher than that of BPA. These results suggest that MPDPB has a strong affinity with BPA.

We further quantitatively analyzed the affinity of MPDPB with BPA by DFT calculation. Notably, the most widely used activated carbon (AC) and β-cyclodextrin-based material (CD) [12] that has the strongest binding affinity to BPA at present were also explored as the reference. Through DFT calculation, the binding energies of graphitized carbon (the active constituent of activated carbon), β-cyclodextrin, and the MPDPB fragment to BPA were simulated (Figure 2(a)–(c)). We found that the binding energy of β-cyclodextrin to BPA is 180% higher than that of activated carbon, consistent with previous reports [25]. Notably, MPDPB has the highest binding energy among these three materials. The binding energy was calculated to be 37.84 kcal/mol (Figure 2(d)), which is five times and 2.3 times that of activated carbon and β-cyclodextrin, respectively. Such high binding energy was primarily ascribed to the increased van der Waals force between MPDPB and BPA as a result of the well-matched pore size of MPDPB (0.59 nm) to BPA, thus contributing to the significantly enhanced affinity.

To further verify the simulation results, Quartz Crystal Microbalance (QCM) measurement was then carried out (Figure 2(e)). By depositing three adsorbents, MPDPB, CD and AC, respectively, on the QCM chip, followed by injecting an extremely low concentration of BPA (0.1 ppb), the adsorption capacity of these three materials was examined *via* monitoring the changes in surface plasmon resonance (SPR) frequency of the gold film on the chip. The mass of the adsorbed BPA can be calculated by the Sauebrey equation [26,27]. As illustrated in Figure 2(f), AC showed a negligible change in SPR frequency, whereas we detected a slight frequency change (0.1 Hz) for β-cyclodextrin, indicating the stronger binding ability of β-cyclodextrin with BPA compared to AC. In sharp contrast, a drastically increased frequency shift was observed for MPDPB (3.7 Hz) upon injection with BPA. The adsorption mass was determined to be 9.35 ng/cm^2 according to the Sauebrey equation. More impressively, negligible changes in frequency were observed when BPA was replaced by deionized water. All these results strongly suggested that MPDPB can firmly bind with BPA molecules at extremely low concentrations.

We must realize that the structure of MPDPB is an amorphous structure, but this structure is not all disorderly and chaotic. MPDPB is actually polymerized by the monomer DPB, which possesses a large molecular structure. DPB monomer is composed of three triphenylamine molecules that are easily oxidized and polymerized. Once polymerized, each monomer can be connected with the surrounding 6 DPB monomers to form a structural domain, and the pore diameter

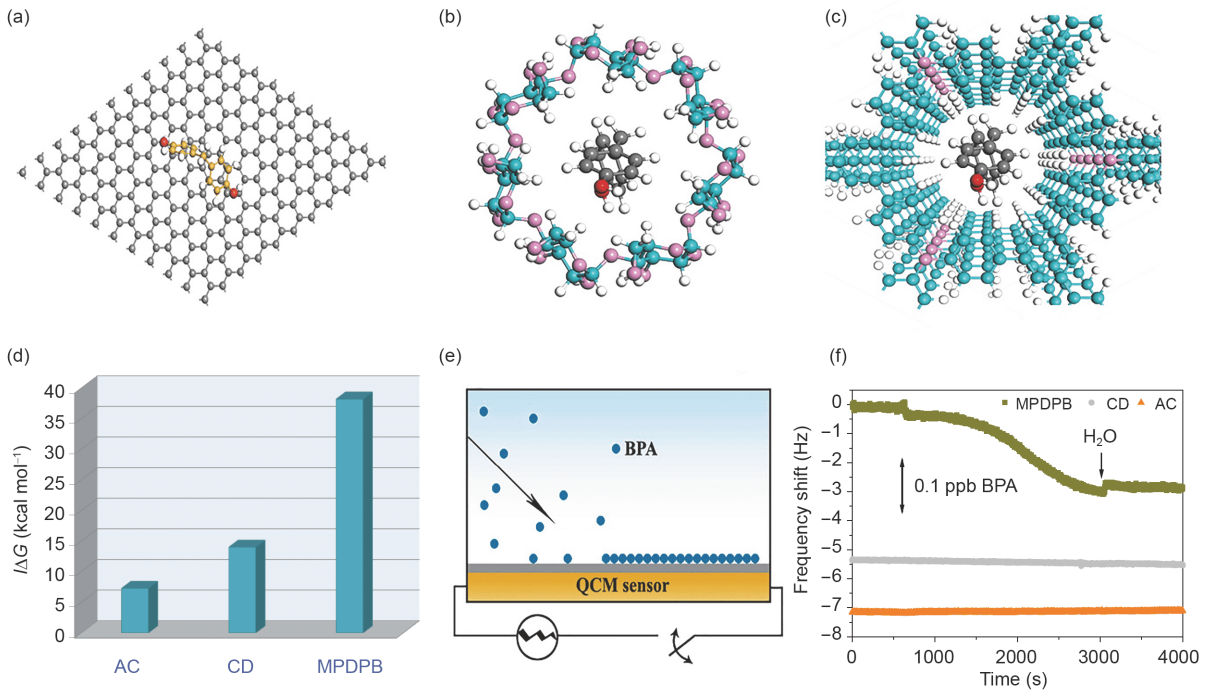

Figure 2 The DFT simulation of the binding sites of AC (a), and β-cyclodextrin (b) for BPA. (c) DFT simulation of the binding sites of MPDPB for BPA. (d) The binding energies of AC, CD, and MPDPB towards BPA. (e) Schematic diagram of the QCM electrode modified by MPDPB for BPA adsorption. (f) Frequency shifts of QCM electrode modified by MPDPB, CD, and AC after injection of 0.1 ppb of BPA (color online).

in this local structural domain is theoretically 0.59 nm. Both of the polymers, PDPB and MPDPB, synthesized by DPB contain the 0.59 nm pore, which further confirms the polymerization process. We have also determined through QCM that BPA could be adsorbed firmly by MPDPB, while AC and CD without 0.59 nm pores are difficult to achieve. Based on this, we believe that MPDPB could adsorb BPA effectively.

3.3 Stability of MPDPB in the water environment

For practical applications, the adsorbent must have a high tolerance to changes in the water environment such as acid, alkaline, salt concentration, and high temperature. Unlike many currently developed adsorbents that generally contain coordination bonds, such as MOF, COF and, other new adsorbents, MPDPB was completely composed of stable chemical bonds, as verified by XPS analysis and nuclear magnetic analysis (Figures S6, S7, Figure 3(a)). Through TGA, we found that MPDPB has very high thermal stability. In the air, only about 547 °C can it be completely decomposed (Figure S11). These stable chemical bonds were found to be thermally stable without any change of morphology and structure after heating at a high temperature of 300 °C for 8 h as illustrated by SEM imaging (Figure 3(b)). Even after having been immersed in acid (pH 4), alkali (pH 10) and high salt (1 M NaCl) for 7 days, no morphology or structure changes were found (Figure S12 and Figure 3(c)), clearly suggesting the high stability of MPDPB and its great potential for practical applications.

3.4 Adsorption efficiency of MPDPB for BPA

We evaluated the adsorption capacity of MPDPB towards BPA in an aqueous solution to demonstrate the potential of MPDPB for BPA removal. At an adsorbent mass of 1 mg/mL and an initial concentration of BPA 22.8 ppm, MPDPB was much faster in absorbing BPA than the other three materials (Figure S13). Within one minute, 98% of BPA could be removed from the water. One minute after MPDPB treatment, the residual BPA was 0.456 ppm (Figure S14), which is much lower than those when the other three materials were used as the absorbent (1.83 ppm for CD, 2.07 ppm for PDPB, and 15.89 ppm for AC). By investigating the completion time of adsorption equilibrium, we found that MPDPB reached equilibrium in only 5 min, much less than that of the CD, PDPB and AC (Figure S15). When the adsorption reached equilibrium, the residual concentration of BPA after MPDPB treatment was only 0.1 ppm, 11 times and 280 times lower than that of CD and AC, respectively (Figure S16).

It is undeniable that the polymer MPDPB we designed and synthesized can effectively adsorb PBA. In addition to matching the size of the BPA molecule, other key factors affecting adsorption performance are multi-stage pores, large

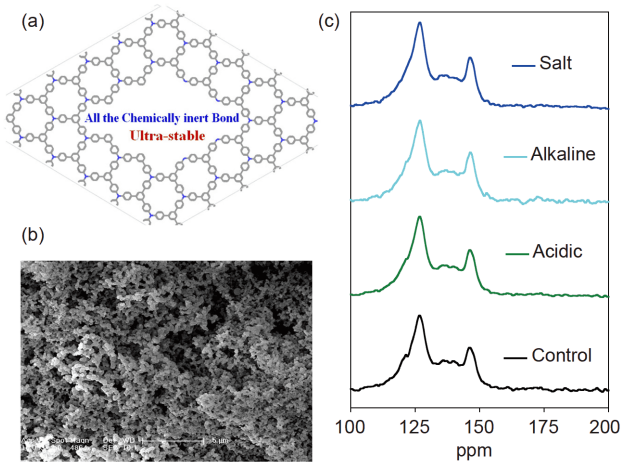

Figure 3 (a) Molecular structure diagram of MPDPB. (b) SEM image of MPDPB. (c) Solid-state NMR spectra of MPDPB before and after being immersed in acidic, alkaline, and high salt solution for 7 days (color online).

specific surface area and pore volume. The Brunauer-Emmett-Teller (BET) surface area and pore volume of MPDPB are almost two and three times that of PDPB, respectively. Moreover, an abundant multi-stage pore structure is demonstrated by MPDPB. Therefore, MPDPB illustrates better adsorption performance than PDPB. In fact, it is difficult to identify that all of the BPA is absorbed into the small pore. It is certain that some of the bisphenol A is adsorbed into the pore of 0.59 nm, and some of it is adsorbed into other larger pores. MPDPB is an amorphous structure, and most of the pores are larger than 0.59 nm, so some of the bisphenol A is adsorbed into the larger pores.

As shown in Figure S17, the BET surface area of MPDPB was decreased after adsorption. Moreover, the pores of 0.59 nm almost disappear, while the pores of 1–2 nm decrease greatly, and the pores of 2–20 nm also decrease to a certain extent. However, we found that the BET surface area and pore size of BPA were recovered after washing BPA with methanol. The above experiments show that the main function of MPDPB in the adsorption process is the small pore size, especially the pore size of 0.59 nm has the strongest adsorption capacity, while the pore size of 2–20 nm can adsorb a certain amount of BPA, but the adsorption capacity is not as strong as the small pore size. Collectively, these results strongly indicated that the high affinity of MPDPB for BPA and its multi-stage porous structure property contribute to the greatly improved adsorption performance.

Encouraged by the ultra-high and fast adsorbing performance of MPDPB, we proceeded to analyze its adsorption rate kinetics, partition coefficient, and maximum adsorption capacity, which are the three most important parameters in determining the feasibility of the adsorbent for practical applications. We found that the adsorption of BPA by MPDPB coincided with pseudo-secondary kinetics, indicating that its adsorption was mainly ascribed to physical adsorption (Figure S18). Consistent with the simulation results, the pseudo-second-rate constant (K_{obs}) for MPDPB towards BPA was determined to be 4.85 g/(mg min) (Figure 4(a)), almost three times that of CD adsorbent (1.65 g/(mg min)), and two orders of magnitude of AC. On the other hand, the value of the partition coefficient represents the affinity of one adsorbent, and is thus a significant parameter for the performance metrics of the adsorbent. When a certain amount of adsorbent is added to a certain concentration of pollutant aqueous solution, the pollutant enters into the adsorbent from the water body and redistributes between the water body and the adsorbent. The partition coefficient (K_d) is used to investigate the distribution of pollutant adsorbent and water when the adsorption equilibrium is reached. According to the experimental part (2.11), we can directly measure the K_d value. Generally, adsorbents with a K_d value above 1.0×10^5 mL/g typically have a good adsorption performance [28,29]. In the case of BPA, there is currently no such adsorbent. Impressively, MPDPB has shown a higher K_d value up to 2.27×10^5 mL/g (Figure 4(b)), much higher than those of CD, PDPB and AC without mesoporous structure (2.06×10^4, 5.6×10^4 and 6.6×10^3 mL/g, respectively), providing further evidence for the better adsorption performance of MPDPB. Also, MPDPB exhibited a maximum adsorption capacity of 826 mg/g (Figure S19), which is the highest value among the reported literature (Figure S20) [12,29–32]. Regardless, three important figures of merits, K_{obs}, K_d, and q_{max} of MPDPB are determined to be one of the highest among currently studied BPA absorbents (Table 1) [10,12,18,30–35].

Next, long-term stability tests were further carried out by immersing MPDPB in actual seawater (high salt), acidic water (pH 4) and alkaline water (pH 10) for 7 days. Encouragingly, there was no decay on the BPA removal efficacy (Figure 4(c)). We also investigated the removal efficiency of BPA under different pH conditions. We found that in acidic conditions, N protonation in MPDPB would lead to a slight decrease in adsorption performance, while in alkaline conditions, BPA de-protonation would also lead to a decrease in removal efficiency. In order to investigate the effect of ions on the adsorption of BPA in natural water, we used lake water from the South Lake of Changchun to test the adsorption of BPA. We found that in real water, the removal efficiency of BPA was almost not affected, and the removal efficiency was still as high as 99.3% (Figure S21). Added to this, recycling of MPDPB could be achieved by simply washing with methanol at room temperature, which is more convenient as compared with complicated energy-intensive processes for AC regeneration. After five consecutive adsorption and desorption cycles, MPDPB did not show an obvious loss of absorbing performance (Figure S22).

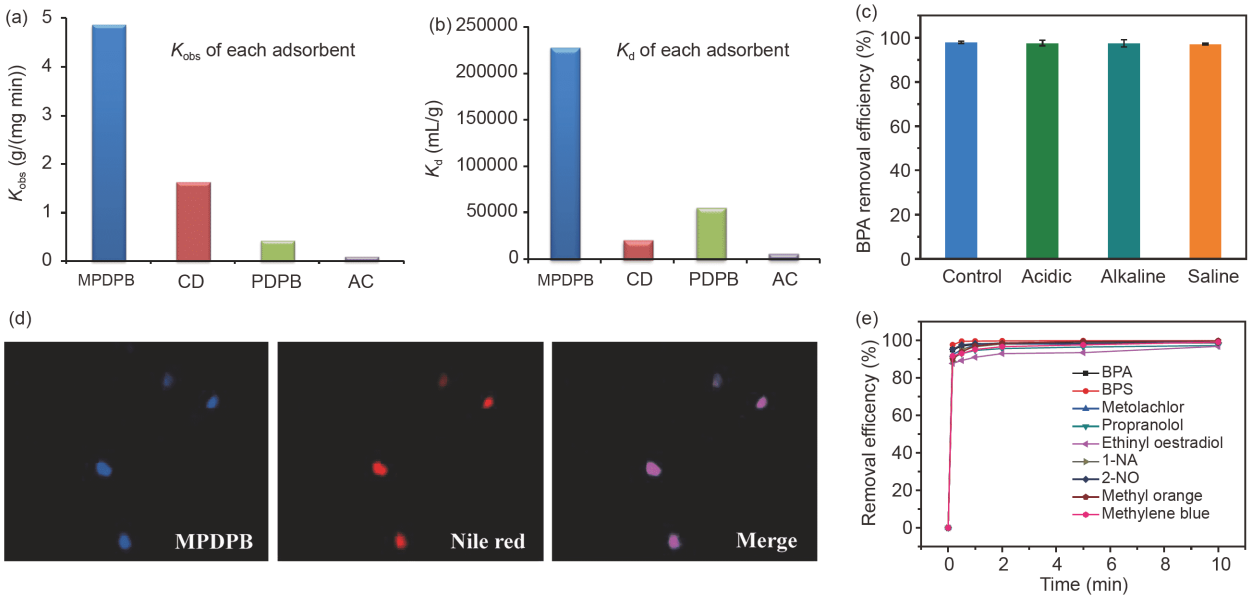

Figure 4 K_{obs} (a) and K_d (b) values for MPDPB, CD, PDPB, and AC, respectively. (c) BPA (0.1 mM) removal efficiency of MPDPB (1 mg/mL) under different conditions. (d) Fluorescence microscopy images of MPDPB, Nile red and MPDPB loaded with Nile red. (e) Time-dependent adsorption efficiency of each organic pollutant by MPDPB (1 mg/mL) (color online).

Table 1 BPA removal performance of variously reported adsorbents

Reference	Materials	Removal rate at equilibrium (%)	Q_{max} (mg/g)	K_d (mL/g)	K_{obs} (g/(mg min))
Our work	MPDPB	99.5	826	2.27×10^5	4.86
[17]	P-Ppy(AOT)	68.8	–	2.2×10^3	–
[18]	Supramolecular absorbents	90	–	3×10^4	–
[11]	Nanoparticles	77	–	8.4×10^2	–
[10]	Covalent organic framework	80	–	4×10^3	182.3
[12]	Porous β-cyclodextrin polymer	95	88	2.06×10^4	1.65
[30]	Phenolation of cyclodextrin polymers	82	250	5.02×10^3	1.61
[34]	MoS_2-CD polymer	93.2	–	1.5×10^4	–
[31]	Porous hybrid materials	95.4	157.4	–	–
[35]	Porous β-cyclodextrin copolymer	87.7	258	–	0.109
[33]	Pillar[5]larene-based 3D network polymer	62.1	68.5	1.62×10^3	–
[32]	Crosslinked-cyclodexrin polymer	93	139.1	–	–

3.5 Adsorption efficiency of MPDPB for other small organic molecular pollutants

In addition to BPA, there are a large number of small organic molecular pollutants commonly exist in water, posing a significant threat to the environment and human health [11,36]. Recently, MOF materials with large specific surface areas have been used to treat one sort of organic pollutant in water, and good results have been achieved [37–42]. However, this porous material with a single pore size can hardly deal with the treatment of small organic pollutants with different molecular sizes. Since MPDPB has a multi-stage porous structure, we hypothesized that the size-matched adsorption strategy mediated by MPDPB could be extended to effective adsorption of other common organic small molecule pollutants with different sizes, similar to the case of BPA. We tested the common contaminantsin water resources to verify our hypothesis. Firstly, we investigated the MPDPB adsorption of Nile red dye. We can use fluorescence microscopy to detect the adsorption of Nile red by MPDPB *in situ* thanks to MPDPB itself having strong fluorescence characteristics. Under the excitation of ultraviolet light, MPDPB exhibits intense blue fluorescence. Once there is the existence of Nile red in the aqueous solution, it is completely absorbed into MPDPB (Figure 4(d)). The experiment demonstrated that MPDPB could effectively adsorb Nile red

dye pollutants in water. We further extend MPDPB to the removal of common small molecular organic pollutants in other water bodies (Figure S23). Results showed that MPDPB demonstrated fast and high absorbing capacities toward these contaminants comparable to that of BPA (Figure S24). Notably, 91.1%–99.7% of BPS, metolachlor, propranolol, 1-naphthylamine, 2-naphthol, methyl orange and methylene blue could be removed within 1 min by MPDPB (Table S1, Supporting Information online). The slightly lower removal efficiency of ethinyl oestradiol (91.1%) at one minute was presumably ascribed to its larger size and electrical neutrality. Since BPS has a similar size and molecular structure to BPA, it is thus unsurprising that MPDPB demonstrated the highest removal rate of BPS (99.7%) at one minute among these pollutants. The removal of these pollutants could be completed within 10 min. Impressively, the removal efficiency of these pollutants ranged from 97.3% to 99.8% is achieved. It is noteworthy that the removal efficiency of ethinyl oestradiol has also been greatly improved, reaching 97.6% after 10 min of equilibrium (Figure 4(e)). Compared with other small molecule pollutants, the transport efficiency of large size pollutants in MPDPB is lower, such as small molecule pollutants. The above experiments fully show that MPDPB can adsorb many other small molecular organic pollutants with different molecular sizes efficiently, which is mainly due to the multi-stage pore structure and conjugated structure of MPDPB.

3.6 Removal of BPA through the MPDPB composite columns and filter membranes

Another important factor that must also be taken into consideration when developing new adsorbents relates to the environmental biocompatibility of the adsorbent itself. To evaluate the toxicity of MPDPB, we investigated the cytotoxicity of MPDPB *via* incubating 0.25–2 mg/mL of MPDPB with human breast cells (HeLa Cells). After incubation for 24 h, the cell viability was quantified by MTT assay, and the result showed that more than 90% of cells treated with MPDPB remained alive even at a high concentration of 2 mg/mL (Figure 5(b)), indicating the good biocompatibility of MPDPB. The cell viability was also determined using calcein AM and propidium iodide (PI) dual staining. As shown in Figure 5(a), few dead cells were found after incubation of 2 mg/mL of MPDPB for 24 h. The above experiments fully demonstrate that MPDPB has good biocompatibility.

The development of a point-of-use device for ultrafast water purification is of great significance. Thus, MPDPB was dispersed in ethanol (5 mg/mL), and then coated onto the medical non-woven fabric, followed by drying for large-scale preparation of non-woven fabric-based MPDPB adsorption filter, with a loading amount of 50 mg/g. Through SEM, we found that MPDPB particles were successfully loaded on non-woven fabrics (Figure 5(c)). Moreover, this convenient method can be used to prepare large-sized MPDPB loaded non-woven fabrics (Figure 5(d)). Further XPS analysis of non-woven fabrics loaded with MPDPB showed that compared with non-woven fabrics without MPDPB, there was an obvious N peak (Figure S25). This is because non-woven fabrics contain very little N element, and the N element comes from MPDPB. Further detailed analysis of the N element in MPDPB revealed that it was derived from tertiary amine in MPDPB (Figure S26). This shows that MPDPB can be effectively loaded onto the non-woven fabric in this simple way. Using this MPDPB-based non-woven fabric filter and polypropylene (PP) cotton, we built a water purifier column to purify the wastewater sample containing 20 ppm BPA. As expected, an ultra-high BPA absorbance rate of 99.8% was achieved (Figure 5(e)). For comparison, a BPA absorbance rate of only 8% was obtained through a water purifier consisting of non-woven fabric and PP cotton, illustrating the high affinity of MPDPB to BPA enabled BPA molecules to be efficiently trapped in the MPDPB-based non-woven fabric. Furthermore, 10 mg MPDPB was loaded on a nonwoven fabric with a diameter of 3 cm and then integrated into the bottle cap to form a simple filter, which could rapidly remove 95.2% of BPA from the wastewater (Figure 5(f)). The MPDPB filter is easy to carry and low cost, so it is expected to be widely used in low-income areas (which are often heavily affected by water pollution). In many cases, the concentration of these small organic pollutants in water is extremely low, so it is very difficult for conventional adsorbents to treat this water sample. Here we try to use the MPDPB water filter to treat the wastewater containing many kinds of low concentrations of organic pollutants. The water samples before and after treatment were analyzed by HPLC-MS. The experimental results demonstrated that most of the pollutants could be effectively removed *via* the simple filter, and successfully reduce the contaminants down to a safe level (Table S2). The long-term stability of MPDPB-based non-woven fabric was firstly explored by comparing the SEM images before and after storage for one month in the deionized water. As expected, no morphological changes were observed, and the MPDPB particles were still firmly fixed on the cloth (Figures S27, S28). Moreover, there is almost no difference in removal efficiency for BPA before and after storage, consisting well with the acquired SEM images.

4 Conclusions

In summary, we have presented a molecular structure-derived design and development of a novel MPDPB porous polymer-based absorbent for ultrafast and highly efficient

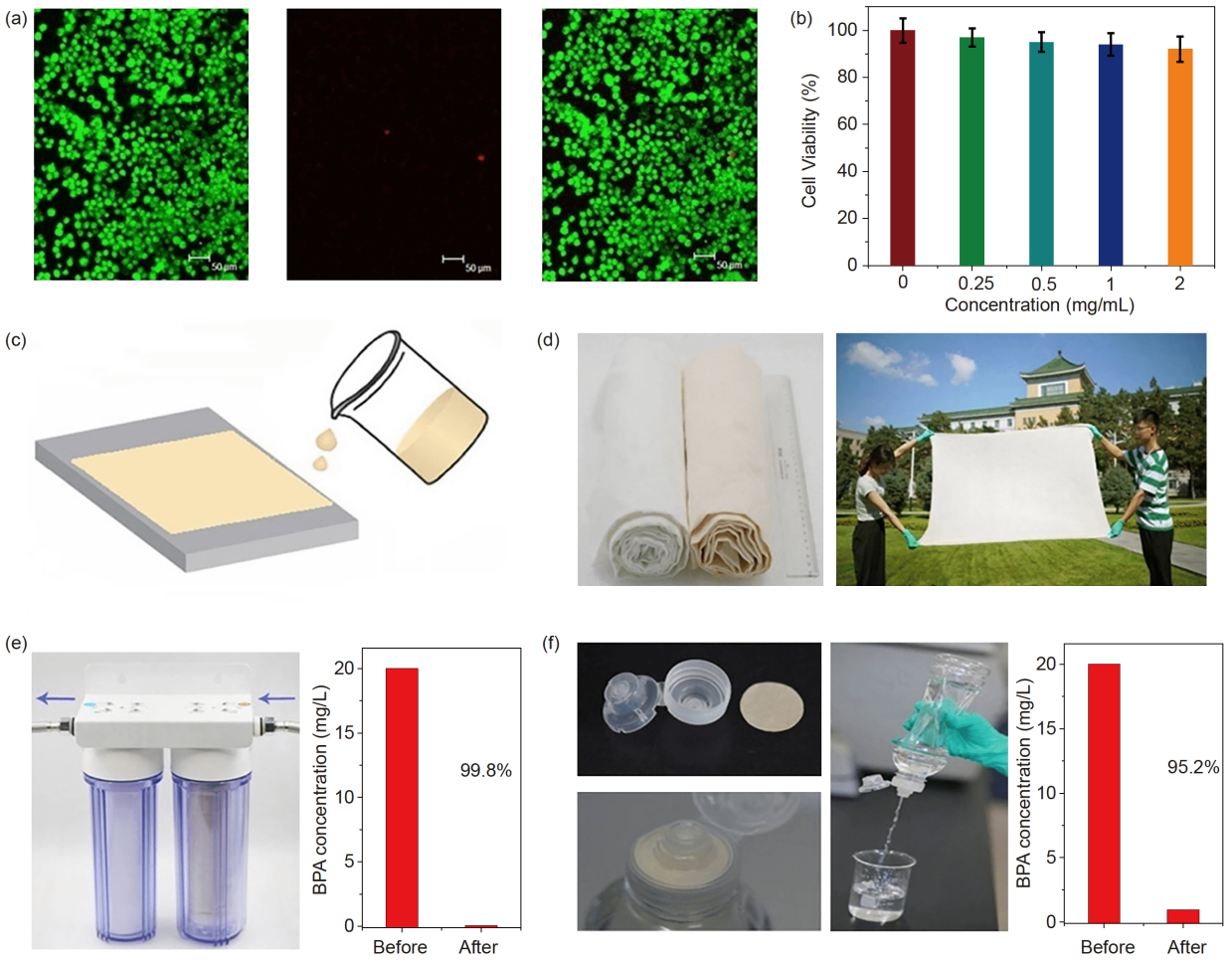

Figure 5 (a) Confocal imaging of calcein AM (green, live cells) and propidium iodide (red, dead cells) co-stained HeLa cells after incubation of MPDPB at a concentration of 2 mg/mL. (b) Cell viability of HeLa cell after incubation of MPDPB with various concentrations for 24 h. (c) Schematic illustration of the preparation of MPDPB-based non-woven fabric. (d) Photograph of the non-woven fabric and MPDPB-based non-woven fabric. (e) Point-of-use device based on MPDPB for wastewater treatment (left) and the BPA concentration before and after treatment (right). (f) Photograph of the point-of-use non-woven fabric (left) and its absorption efficiency (right) (color online).

removal of BPA in water. Benefiting from the favorable binding capability to BPA and multi-stage porous structure, MPDPB could effectively eliminate BPA from water, with significantly improved adsorption kinetics, partition coefficient and maximum adsorption amount, compared with currently investigated absorbents. Meanwhile, MPDPB has also demonstrated robust adsorption capability towards many other organic contaminations in water. Moreover, the molecular structure of MPDPB was chemical inertia and highly tolerant of harsh environments, contributing to the high adsorption stability under acidic, alkaline and high salt conditions. It is also worth noting that MPDPB could be easily processed to adsorption filters on a large scale for more convenient water purification, with a high removal efficacy of BPA up to 99.8%. We believe that the proposed material design derived from the specific structure of the contaminant molecule can be extended to exploring further innovative adsorption materials to efficiently remove a wide range of water pollutants for broad water purification.

Acknowledgements This work was supported by the National Key Research and Development Program of China (2016YFA0203200), the National Natural Science Foundation of China (21635007, 21974134), K. C. Wong Education Foundation and Computing Centre of Jilin Province.

Conflict of interest The authors declare no conflict of interest.

Supporting information The supporting information is available online at http://chem.scichina.com and http://link.springer.com/journal/11426. The supporting materials are published as submitted, without typesetting or editing. The responsibility for scientific accuracy and content remains entirely with the authors.

1 Landrigan PJ, Fuller R, Acosta NJR, Adeyi O, Arnold R, Basu NN, Baldé AB, Bertollini R, Bose-O'Reilly S, Boufford JI, Breysse PN, Chiles T, Mahidol C, Coll-Seck AM, Cropper ML, Fobil J, Fuster V, Greenstone M, Haines A, Hanrahan D, Hunter D, Khare M, Krupnick A, Lanphear B, Lohani B, Martin K, Mathiasen KV, McTeer MA, Murray CJL, Ndahimananjara JD, Perera F, Potočnik J, Preker AS,

Ramesh J, Rockström J, Salinas C, Samson LD, Sandilya K, Sly PD, Smith KR, Steiner A, Stewart RB, Suk WA, van Schayck OCP, Yadama GN, Yumkella K, Zhong M. *Lancet*, 2018, 391: 462–512
2 Jiang D, Chen WQ, Zeng X, Tang L. *Environ Sci Technol*, 2018, 52: 3706–3715
3 Barrios-Estrada C, de Jesús Rostro-Alanis M, Muñoz-Gutiérrez BD, Iqbal HMN, Kannan S, Parra-Saldívar R. *Sci Total Environ*, 2018, 612: 1516–1531
4 Borrell B. *Nature*, 2010, 464: 1122–1124
5 Kaiser J. *Science*, 2007, 317: 884a–885a
6 McDonald GR, Hudson AL, Dunn SMJ, You H, Baker GB, Whittal RM, Martin JW, Jha A, Edmondson DE, Holt A. *Science*, 2008, 322: 917
7 Moreman J, Takesono A, Trznadel M, Winter MJ, Perry A, Wood ME, Rogers NJ, Kudoh T, Tyler CR. *Environ Sci Technol*, 2018, 52: 6656–6665
8 Zimmerman JB, Anastas PT. *Science*, 2015, 347: 1198–1199
9 Jin H, Zhu J, Chen Z, Hong Y, Cai Z. *Environ Sci Technol*, 2018, 52: 812–820
10 Karak S, Dey K, Torris A, Halder A, Bera S, Kanheerampockil F, Banerjee R. *J Am Chem Soc*, 2019, 141: 7572–7581
11 Brandl F, Bertrand N, Lima EM, Langer R. *Nat Commun*, 2015, 6: 7765
12 Alsbaiee A, Smith BJ, Xiao L, Ling Y, Helbling DE, Dichtel WR. *Nature*, 2016, 529: 190–194
13 Zbair M, Ainassaari K, Drif A, Ojala S, Bottlinger M, Pirilä M, Keiski RL, Bensitel M, Brahmi R. *Environ Sci Pollut Res*, 2018, 25: 1869–1882
14 Wang Y, Zeiri O, Raula M, Le Ouay B, Stellacci F, Weinstock IA. *Nat Nanotech*, 2017, 12: 170–176
15 Byun J, Patel HA, Thirion D, Yavuz CT. *Nat Commun*, 2016, 7: 13377
16 Wu J, Xu F, Li S, Ma P, Zhang X, Liu Q, Fu R, Wu D. *Adv Mater*, 2019, 31: 1802922
17 Ren Y, Lin Z, Mao X, Tian W, Van Voorhis T, Hatton TA. *Adv Funct Mater*, 2018, 28: 1801466
18 Xie S, Wu S, Bao S, Wang Y, Zheng Y, Deng D, Huang L, Zhang L, Lee M, Huang Z. *Adv Mater*, 2018, 30: 1800683
19 Schmidt BVKJ, Barner-Kowollik C. *Angew Chem Int Ed*, 2017, 56: 8350–8369
20 Alzate-Sánchez DM, Ling Y, Li C, Frank BP, Bleher R, Fairbrother DH, Helbling DE, Dichtel WR. *ACS Appl Mater Interfaces*, 2019, 11: 8089–8096
21 Liu X, Pang H, Liu X, Li Q, Zhang N, Mao L, Qiu M, Hu B, Yang H, Wang X. *Innovation*, 2021, 2: 100076
22 Plater MJ, McKay M, Jackson T. *J Chem Soc Perk T 1,* 2000, 2695-2701
23 Feng JK, Cao YL, Ai XP, Yang HX. *J Power Sources*, 2008, 177: 199–204
24 Sun J, Liang Z. *ACS Appl Mater Interfaces*, 2016, 8: 18301–18308
25 Yao N, Zhang X, Yang Z, Yang W, Tian Z, Zhang L. *ACS Appl Mater Interfaces*, 2018, 10: 29083–29091
26 Tu M, Wannapaiboon S, Khaletskaya K, Fischer RA. *Adv Funct Mater*, 2015, 25: 4470–4479
27 Shpigel N, Levi MD, Sigalov S, Girshevitz O, Aurbach D, Daikhin L, Jäckel N, Presser V. *Angew Chem Int Ed*, 2015, 54: 12353–12356
28 Ai K, Ruan C, Shen M, Lu L. *Adv Funct Mater*, 2016, 26: 5542–5549
29 Li B, Zhang Y, Ma D, Shi Z, Ma S. *Nat Commun*, 2014, 5: 5537
30 Klemes MJ, Ling Y, Chiapasco M, Alsbaiee A, Helbling DE, Dichtel WR. *Chem Sci*, 2018, 9: 8883–8889
31 Zhang H, Ma S, Li Y, Ou J, Wei Y, Ye M. *J Hazard Mater*, 2019, 367: 465–472
32 Yang CA, Huang H, Ji T, Zhang KS, Yuan LQ, Zhou CS, Tang KW, Yi JM, Chen XB. *Polym Int*, 2019, 68: 805–811
33 Shi B, Guan H, Shangguan L, Wang H, Xia D, Kong X, Huang F. *J Mater Chem A*, 2017, 5: 24217–24222
34 Liu J, Yang Y, Bai J, Wen H, Chen F, Wang B. *Anal Chem*, 2018, 90: 3621–3627
35 Lu P, Cheng J, Li Y, Li L, Wang Q, He C. *Carbohydrate Polyms*, 2019, 216: 149–156
36 Liang B, Wang H, Shi X, Shen B, He X, Ghazi ZA, Khan NA, Sin H, Khattak AM, Li L, Tang Z. *Nat Chem*, 2018, 10: 961–967
37 Wang B, Lv XL, Feng D, Xie LH, Zhang J, Li M, Xie Y, Li JR, Zhou HC. *J Am Chem Soc*, 2016, 138: 6204–6216
38 Mon M, Bruno R, Tiburcio E, Viciano-Chumillas M, Kalinke LHG, Ferrando-Soria J, Armentano D, Pardo E. *J Am Chem Soc*, 2019, 141: 13601–13609
39 Wang J, Li Z, Wang Y, Wei C, Ai K, Lu L. *Mater Horiz*, 2019, 6: 1517–1525
40 Wang J, Ai K, Lu L. *J Mater Chem A*, 2019, 7: 16850–16858
41 Wang J, Fan D, Jiang C, Lu L. *Nano Today*, 2021, 36: 101034
42 Fan D, Wang J, Wang E, Dong S. *Adv Sci*, 2020, 7: 2001766